J. Fluid Mech. (2009), *vol.* 620, *pp.* 333–352.
doi:10.1017/S0022112008004801 Printed in the United Kingdom

Dynamics of drop coalescence at fluid interfaces

FRANÇOIS BLANCHETTE[1]† AND TERRY P. BIGIONI[2]

[1]School of Natural Sciences, University of California Merced, 5200 N. Lake Road, Merced, CA 95343, USA

[2]Department of Chemistry, University of Toledo, 2801 W. Bancroft Street, Toledo, OH 13606, USA

(Received 10 April 2007 and in revised form 23 September 2008)

Drop coalescence was studied using numerical simulations. Liquid drops were made to coalesce with a body of the same liquid, either a reservoir or a drop of different size, each with negligible impact velocity. We considered either gas or liquid as a surrounding fluid, and experimental results are discussed for the gas–liquid set-up. Under certain conditions, a drop will not fully coalesce with the liquid reservoir, leaving behind a daughter drop. Partial coalescence is observed for systems of low viscosity, characterized by a small Ohnesorge number, where capillary waves remain sufficiently vigourous to distort the drop significantly. For drops coalescing with a flat interface, we determine the critical Ohnesorge number as a function of Bond number, as well as density and viscosity ratios of the fluids. Studying the coalescence of two drops of different sizes reveals that partial coalescence may occur in low-viscosity systems provided the size ratio of the drops exceeds a certain threshold. We also determine the extent to which the process of partial coalescence is self-similar and find that the viscosity of the drop has a large effect on the droplet's vertical velocity after pinch off. Finally, we report on the formation of satellite droplets generated after a first pinch off and on the ejection of a jet of tiny droplets during coalescence of a parent drop significantly deformed by gravity.

1. Introduction

The impact of a drop of fluid onto a reservoir or a second drop has long been a problem of interest to physicists owing to its relevance in raindrops dynamics (Berry & Reinhardt 1974), production of ocean mist and airborne salt particles (Raes *et al.* 2000), foams and emulsions (Bhakta & Ruckenstein 1997) and more generally vorticity generation near an interface through the formation of a vortex ring (Thompson & Newall 1885; Sarpaya 1996; Dooley *et al.* 1997).

Depending on its impact velocity, the drop may either bounce or coalesce or splash as it hits the interface of a liquid reservoir (Cai 1989; Rein 1996; Nietzel & Dell'Aversana 2002). Collisions between drops may also result in temporary coalescence and fragmentation (Orme 1998). When the kinetic energy of the drop is small, the surrounding fluid is slowly expelled from the gap separating the two fluid masses as the drop approaches the second interface. Drops may then appear to 'float' on the interface for a few seconds, as first reported by Reynolds (1881). Several authors have since been interested in this phenomenon and have attempted to measure or calculate the residence time of drops on a horizontal interface (Cockbain & McRoberts 1953; Linton & Sutherland 1956; Charles & Mason 1960a; Gonipath & Koch 2002).

† Email address for correspondence: fblanchette@ucmerced.edu

Eventually, the thickness of the gap of surrounding fluid becomes sufficiently small, between 10 and 100 nm, for van der Waals force to become important, at which point the two interfaces coalesce and the drop comes in contact with the bulk fluid (Hahn, Chen & Slattery 1985). As surface tension acts to minimize the surface energy of the interface, the width of the neck joining the fluid masses progressively widens. Simultaneously, fluid within the drop is accelerated towards the bulk fluid by the surface tension pulling on the top of the drop. This mechanism has been described by early investigators, and the motion of the bulk fluid after coalescence of liquid drops was studied in the 19th century by both Reynolds (1875) and Thompson & Newall (1885) as a source of vorticity.

The coalescence of drops with a flat interface may either result in the total absorption of the drop within the bulk fluid or, alternatively, in the partial coalescence of the drop, thus leaving a smaller drop to rebound on the interface (Charles & Mason 1960*a*). Partial coalescence may occur several times in succession to form what has been termed a coalescence cascade (Thoroddsen & Takehara 2000). This process occurs within a few milliseconds and may be visualized using a high-speed camera. Recently, a possible explanation of the multiple coalescence of drops covered with surfactant has been suggested (Pikhitsa & Tsargorodskaya 2000). However, partial coalescence has been observed even in the absence of surfactants (Thoroddsen & Takehara 2000; Aryafar & Kavehpour 2006; Chen, Mandre & Feng 2006) and a mechanism for such partial coalescence was presented in Blanchette & Bigioni (2006).

When the fluid in which the drop is initially suspended is gaseous, an interesting feature of the coalescence cascade is the large rebound height of the smaller droplet on the interface, which can greatly exceed its initial height. Although the bouncing of drops on super-hydrophobic solid surfaces may exhibit very large restitution coefficients (Richard & Quéré 2000), the rebound of drops on fluid interfaces typically results in large energy loses (Jayaratne & Mason 1964; Bach, Koch & Gonipath 2004). Therefore, drops resulting from partial coalescence must impact the interface with a large velocity in order to reach heights of several times their radius (Honey & Kavehpour 2006).

We present here numerical simulations of the coalescence of a drop with either a horizontal interface or a drop of a different size. Simulations of flows where surface tension plays an important role are notoriously difficult to implement. Because of their relatively low computational requirements, boundary integral methods were first developed and applied to problems where inertia could be neglected (e.g. Pozridkis 1992) or where viscous effects were absent (Longuet-Higgins & Cokelet 1976). Volume of fluids methods capable of incorporating viscous and inertial effects and of solving the full Navier–Stokes equations, with the addition of a local force near the interface modelling surface tension, were later developed (Lafaurie *et al.* 1994). Alternatively, one may keep track of the position of the interface using markers, resulting in better accuracy at the expense of some flexibility (Popinet & Zaléski 1999, 2002). Level set methods (see e.g. Sethian 1999) have also been used successfully to simulate the evolution of fluid interfaces. They require somewhat more complicated implementations but recover the flexibility to handle topological changes (Sussman, Smereka & Osher 1994). For cases where increased resolution may be required in small localized regions of the flow, adaptive meshing near the interface has been used (Notz & Basaran 1999) and may be combined with level set methods (Sussman *et al.* 1999). Reviews of the different numerical approaches to simulations of interfacial flows may be found in Scardovelli & Zaléski (1999) and Osher & Fedkiw (2001).

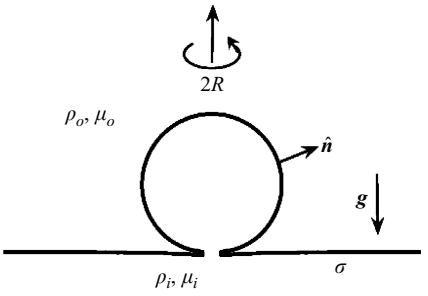

FIGURE 1. Initial conditions of an axially symmetric drop on a flat interface. Coalescence has just begun and the fluid is assumed to be at rest.

We describe the conditions required for a drop to undergo multiple coalescence as it comes into contact with a horizontal surface. Our analysis is based on numerical simulations and experiments where multiple coalescence is observed in detail with a high-speed video camera. We analyse the pinch off mechanism and describe the possible configurations a drop may take after coalescing with a horizontal interface or a second drop. The governing equations and our numerical approach to solving them are described in §§2 and 3, respectively. Our experimental set-up is described in §4 and our numerical results and experimental results are presented in §5, and we conclude with a brief outlook onto future research in §6.

2. Governing equations

We investigate the coalescence of a drop coming slowly into contact with a horizontal interface, as illustrated in figure 1. Fluid in the drop is identical to that in the lower region and will be referred to as the inner fluid; fluid surrounding the drop will be referred to as the outer fluid. Before coalescence is initiated, the outer fluid must be expelled from the gap separating the drop and the interface. Provided the downward velocity of the drop is initially small, coalescence may be delayed for several seconds as the outer fluid drains from the gap (Reynolds 1881; Gonipath & Koch 2001). The drop then essentially comes to rest before coalescence occurs. We study here the evolution of systems where the drop is initially at rest and coalescence is initiated at time $t = 0$.

Both fluids obey the Navier–Stokes equations and are coupled through tangential and normal stress balances at the interface:

$$\rho_i((\boldsymbol{u}_i)_t + \boldsymbol{u}_i \cdot \nabla \boldsymbol{u}_i) = -\nabla P_i + \boldsymbol{g}\rho_i + \mu_i \nabla^2 \boldsymbol{u}_i \tag{2.1}$$

$$\rho_o((\boldsymbol{u}_o)_t + \boldsymbol{u}_o \cdot \nabla \boldsymbol{u}_o) = -\nabla P_o + \boldsymbol{g}\rho_o + \mu_o \nabla^2 \boldsymbol{u}_o \tag{2.2}$$

$$\hat{\boldsymbol{\tau}} \cdot [(\mu_i(\nabla \boldsymbol{u}_i + (\nabla \boldsymbol{u}_i)^T)) - (\mu_o(\nabla \boldsymbol{u}_o + (\nabla \boldsymbol{u}_o)^T))]|_S \cdot \hat{\boldsymbol{n}} = 0 \tag{2.3}$$

$$\hat{\boldsymbol{n}} \cdot [(-P_i \bar{\bar{I}} + 2\mu_i(\nabla \boldsymbol{u}_i + (\nabla \boldsymbol{u}_i)^T)) - (-P_o \bar{\bar{I}} + 2\mu_o(\nabla \boldsymbol{u}_o + (\nabla \boldsymbol{u}_o)^T))]|_S \cdot \hat{\boldsymbol{n}} = -2\sigma\kappa' \tag{2.4}$$

where the subscript t denotes a time derivative, the indices 'i' and 'o' indicate the inner and outer fluids respectively and the position of the interface is denoted by S. Here $\boldsymbol{g}$ is the gravity vector (of magnitude g), $\boldsymbol{u}$ the velocity field, ρ the density, P the pressure, μ the viscosity, σ the surface tension, $\hat{\boldsymbol{\tau}}$ a vector tangent to the interface, $\hat{\boldsymbol{n}}$ the unit normal vector pointing towards the outer phase and κ' the mean curvature of the joined interface (figure 1). Note that the mean curvature is defined as $\kappa' = \nabla_S \cdot \hat{\boldsymbol{n}}$, where $\nabla_S \cdot$ is the divergence operator along the interface (Lafaurie *et al.* 1994). We

assume that no evaporation occurs and that the system is isothermal and free of surfactant, thus ensuring that the interface moves with the fluid and that surface tension is constant along the interface. Moreover, we consider that both fluids are incompressible

$$\nabla \cdot \boldsymbol{u}_i = \nabla \cdot \boldsymbol{u}_o = 0. \tag{2.5}$$

To focus on partial coalescence, we consider systems where surface tension effects are dominant over those of gravity. We thus restrict our attention to systems where the Bond number, defined as $Bo = g(\rho_i - \rho_o)R^2/\sigma$, where R is the initial radius of the drop, is smaller than unity. The Bond number captures the ratio of characteristic gravitational to surface forces. In the absence of a sizeable initial drop velocity and for fluids of relatively low viscosity, the time scale of motion will be dominated by a balance between surface tension and inertial forces $t_n = (\rho_i R^3/\sigma)^{1/2}$ (Thorodssen & Takehara 2000). If, however, viscous effects balance surface tension, a typical time scale of motion is $t_v = R\mu_i/\sigma$. To estimate the relative contributions of the viscous and inertial forces, we consider the Ohnesorge number $Oh = t_v/t_n = \mu_i/(\rho_i R\sigma)^{1/2}$. We will mostly be concerned with cases where $Oh \ll 1$, as they turn out to be the most interesting, and we therefore non-dimensionalize (2.1)–(2.4) using t_n, R and ρ_i as typical time, length and density scales. Note that the Ohnesorge number is analogous to the inverse of the Reynolds number if we consider that a typical velocity is $\tilde{u} = R/t_n \sim (\sigma/(\rho R))^{1/2}$.

To facilitate the numerical resolution of the governing equations, we replace the condition of tangential and normal stress balance on the interface with a localized forcing term acting only on the interface and playing the role of surface tension (Lafaurie *et al.* 1994). We therefore add to the Navier–Stokes equation a term of the form $F(\boldsymbol{x}) = \sigma\kappa'\hat{\boldsymbol{n}} \int_S \delta_3(=\boldsymbol{x} - \boldsymbol{x}_0)\,\mathrm{d}\boldsymbol{x}_0$, where δ_3 is a Dirac delta function of dimension 3 and the integral is taken on the interface. This forcing term is then effectively a delta function of dimension 1 which is non-zero on the interface only. In the absence of surface tension gradients, $F(\boldsymbol{x})$ corresponds to purely normal forcing. Using this formulation has the advantage of replacing complicated boundary conditions with an advection equation and a forcing term while preserving the validity of the momentum equation. The interface is then simply advected by the fluid.

We also introduce a volume of inner fluid function, C, such that $C = 0$ in the outer fluid and $C = 1$ in the inner fluid. This allows us to introduce a fluid density and viscosity valid everywhere in our system: $\rho' = \rho_o + C(\rho_i - \rho_o)$ and $\mu' = \mu_o + C(\mu_i - \mu_o)$, respectively. We may then rewrite (2.1)–(2.5) in non-dimensional form as

$$\rho(\boldsymbol{u}_t + \boldsymbol{u} \cdot \nabla \boldsymbol{u}) = -\nabla P + \nabla \cdot (\mu(\nabla \boldsymbol{u} + (\nabla \boldsymbol{u})^T)) + \sigma\kappa\delta_s\hat{\boldsymbol{n}} + CBo\hat{\boldsymbol{g}}, \tag{2.6}$$

$$S_t = \boldsymbol{u}, \tag{2.7}$$

$$\nabla \cdot \boldsymbol{u} = 0, \tag{2.8}$$

where $\hat{\boldsymbol{g}}$ is a unit vector in the direction of gravity, $\kappa = \kappa' R$ is the non-dimensional curvature and we defined $\rho = (1 - C)/\alpha + C$ and $\mu = (1 - C)/\lambda + C$, with $\alpha = \rho_i/\rho_o$ and $\lambda = \mu_i/\mu_o$, the density and viscosity ratios, respectively.

3. Numerical model

In order to effectively solve (2.6)–(2.8), we exploit the axial symmetry of our system and neglect angular dependencies. The interface can then be represented by a one-dimensional curve, thus eliminating complications arising from tracking two-dimensional surfaces. It is known that, at least in liquid–liquid systems, the film of

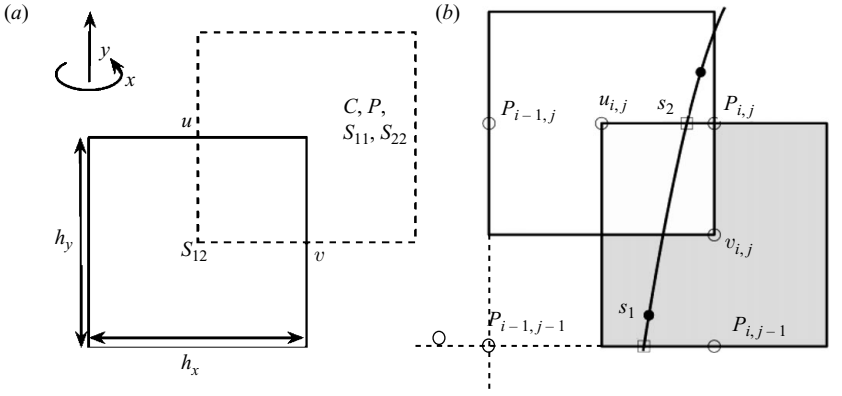

FIGURE 2. (*a*) Our numerical simulations are performed on a staggered grid and boundaries are made to coincide with the dashed lines. Components of the deviatoric stress tensor are defined as $S_{11} = \mu u_x$, $S_{22} = \mu v_y$ and $S_{12} = (1/2)\mu(u_y + v_x)$. (*b*) The interface is represented as a cubic spline interpolation between markers (s_1, s_2, etc).

outer fluid typically ruptures off centre, which generates temporarily asymmetrical flows (Charles & Mason 1960*b*). The initial neck very quickly extends in all directions, however, which brings the flow to near symmetry. Comparisons with experiments (Blanchette & Bigioni 2006) confirmed that while our assumption of axial symmetry does not always allow us to precisely model the very early stages of coalescence, our model accurately captures the later developments of the flow. In particular, the subsequent pinch off that sometimes occurs and leads to multiple coalescence is well reproduced.

We use a classic marker and cell (MAC) algorithm to solve the Navier–Stokes equations and we additionally take special care in estimating the forces and pressure near the interface. Following previous authors (Peyret & Taylor 1983), we solve (2.6) by discretizing the spatial domain into a fixed, Cartesian staggered grid as shown in figure 2(*a*). The surface force is treated separately as explained below. Derivatives are computed using centred differences and the equations are marched forward in time using a backward Euler method. At each time step, we first find a temporary velocity field $\boldsymbol{u}^*$ by ignoring the pressure term. The nonlinear terms in the momentum equations are calculated via an upwinding scheme and the viscous terms using centred differences. We then find the actual velocity by adding the pressure term (Lafaurie *et al.* 1994):

$$\boldsymbol{u}(t + \Delta t) = \boldsymbol{u}^*(t + \Delta t) - \frac{\Delta t}{\rho}\nabla P(t + \Delta t), \tag{3.1}$$

where P is chosen via a a projection method (Brown, Cortez & Minion 2001) so as to render the velocity field solenoidal, and therefore satisfies a Poisson-type equation

$$\nabla \cdot \left(\frac{\Delta t}{\rho}\nabla P(t + \Delta t)\right) = \nabla \cdot \boldsymbol{u}^*(t + \Delta t). \tag{3.2}$$

Equation (3.2) is solved using a multigrid iterative algorithm (e.g. Briggs 1987). This method first solves (3.2) iteratively on a coarse grid by discretizing both sides of the equation using centred differences. The grid is then progressively refined and one iteration of the iterative scheme is computed for each new grid refinement. This algorithm was found to perform well despite abrupt density variations, provided the density ratio was kept at or below 100, as is detailed below.

We keep track of the position of the interface by advecting markers using a first-order Euler method. The position of the interface between markers is interpolated by parameterizing the curve by its arclength s and using cubic splines in x and y. The interface is then differentiable at least once everywhere. To prevent accumulation of markers, we redistribute them evenly after each time step. We note that this redistribution may actually be done less frequently; simulations performed while redistributing markers every 10 time steps yielded results that were virtually identical to those obtained with markers redistributed at every step.

To compute the force due to surface tension, we utilize an axisymmetric version of the algorithm presented by Popinet & Zaléski (1999). To calculate the horizontal and vertical contributions of the surface tension force, we integrate the term $\kappa\delta_s\hat{\boldsymbol{n}}$ over a rectangle of width h_x and height h_y centred at the point where u and v are defined, respectively, as shown in figure 2(b). Integrating over a delta function located on the interface is equivalent to performing a line integral along the portion of the interface that is inside each grid cell, between $s=s_1$ and $s=s_2$ in figure 2(b). The curvature term then becomes

$$\boldsymbol{T} = \int_{s_1}^{s_2} \kappa\hat{\boldsymbol{n}}\,\mathrm{d}s = \left(\frac{\mathrm{d}x}{\mathrm{d}s}, \frac{\mathrm{d}y}{\mathrm{d}s}\right)\bigg|_{s_2} - \left(\frac{\mathrm{d}x}{\mathrm{d}s}, \frac{\mathrm{d}y}{\mathrm{d}s}\right)\bigg|_{s_1} + \int_{s_1}^{s_2} \frac{1}{x}\frac{\mathrm{d}y}{\mathrm{d}s}\left(-\frac{\mathrm{d}y}{\mathrm{d}s}, \frac{\mathrm{d}x}{\mathrm{d}s}\right)\mathrm{d}s. \quad (3.3)$$

Here the first two terms on the right-hand side account for the two-dimensional curvature while the remaining integral describes the radial curvature. The latter integral is evaluated numerically via a trapezoidal method, except at the symmetry axis where the mean curvature is twice the two-dimensional curvature of the curve $(x(s), y(s))$. Finally, to define the surface force at a point, we divide $\boldsymbol{T}$ by the area over which integration was performed. In our numerical scheme, we therefore obtain $\kappa\delta_s\hat{\boldsymbol{n}} = \boldsymbol{T}/(h_x h_y)$. It is worth noting that both the radial and the two-dimensional curvature are required to observe pinch off. The former provides the inward forces generating pinch off from a nearly cylindrical drop, while the latter allows the initial opening of the neck joining drop and reservoir.

Knowing the precise position of the interface also allows us to accurately locate pressure jumps across the interface. For example, to calculate the vertical pressure gradient centred at $v_{i,j}$ in figure 2(b), we again consider the integral of $\partial P/\partial y$ over a grid cell centred on $v_{i,j}$. The pressure on either side of the interface is assumed to be that at the nearest grid point on that same side of the interface, and we find (see Popinet & Zaléski 1999 for more details)

$$\begin{aligned} IP_{i,j} &= \int_{v_{i,j}} \frac{\partial P}{\partial y}\,\mathrm{d}x\,\mathrm{d}y \approx \int_{x_i}^{x_{i+1}} P_j - P_{j-1}\,\mathrm{d}x \\ &\approx P_{i-1,j}(x(s_2) - x_i) + P_{i,j}(x_{i+1} - x(s_2)) \\ &\quad - P_{i-1,j-1}(x(s_1) - x_i) + P_{i,j-1}(x_{i+1} - x(s_1)). \end{aligned} \quad (3.4)$$

In the discretized equations, we may then replace a classical finite difference approximation of $\partial P/\partial y$ with $IP/(h_x h_y)$. Pressure gradients near the interface are therefore computed much more accurately than in methods where the interface is smeared. Because such methods do not track the position of the interface but rather the volume fraction occupied by one fluid in each cell, they have the inconvenience of generating artificial currents with typical velocity $u_a \sim 0.005\sigma/\mu$ (Lafaurie *et al.* 1994). Using the pressure correction described above virtually eliminates such artificial currents.

For grid cells in the proximity of the interface, the local density and viscosity is obtained from the volume fraction of inner fluid, C. Rather than computing the evolution of C as a quantity transported by the fluid, we use the position of the interface to determine at each time step the fraction of each grid cell occupied by the inner fluid. The volume of inner fluid in each cell is found by discretizing the portion of the interface within each cell in $N = 100$ parts and summing the volume between the interface and the boundary of the cell using the method of cylindrical shells. Conservation of mass is therefore not directly enforced, but we find that a resolution of approximately 40 grid points per non-dimensional unit length is sufficient to conserve mass to an accuracy better than 1 %.

Because the position of the interface is tracked with markers, topological changes such as coalescence or pinch off must be handled explicitly. We only allow pinch off to occur at the rotation axis. We define a critical radius r_c such that pinch off occurs when the axial position of the interface becomes less than r_c. We then split the original surface into two disjoined interfaces, which we separate by half a cell width. Coalescence may be handled in a similar manner, by merging two interfaces that come within a given distance of each other. For drops larger than 1 micron, our code cannot accurately determine when coalescence occurs because the thickness of the film of outer fluid may be several orders of magnitude smaller than the drop itself, and cannot be resolved. We focus here on the dynamics of motion starting immediately after coalescence has been initiated and do not attempt to capture the onset of coalescence.

Our simulations are initiated with fluid at rest everywhere and with the drop connected to the lower interface through a thin neck, as shown in figure 1. Unless otherwise stated, we consider that the drop is initially spherical and that the interface is horizontal and planar. The boundary conditions associated with this formulation have the advantage of not involving any free boundaries: we only require no-slip on the bounding walls, i.e. $\boldsymbol{u} = 0$, and symmetry about the rotation axis. The position of the interface at the walls is therefore pinned. In theory, the interface should be allowed to move along the wall through a moving contact line. However, in the cases we are interested in, the side walls are positioned sufficiently far from the drop so as to play no dynamical role. In particular, capillary waves reflected at the boundaries never come into play provided the width of the domain is six non-dimensional units or larger. The boundaries of our domain are made to coincide with the dashed grid of figure 2(a) so that no values of the pressure or stress need to be imposed at the boundary. Velocities normal to the boundaries are directly set to zero. At no-slip boundaries, tangential velocities are made to be zero by adding a point outside the physical domain where the tangential velocity is equal and opposite to that just inside the boundary. At the rotation axis, the tangential stress is set to zero.

4. Experimental set-up

Coalescence events were observed experimentally in an air–liquid system for a range of Bond numbers and Ohnesorge numbers, as determined by the drop size, density, viscosity and surface tension. We studied drops as large as allowed by their stability under gravitational effects, so that $Bo < 1$. Drops were thus nearly spherical at the onset of coalescence. The imaging of small drop sizes was limited by the camera resolution, but drops as small as $\sim 60\,\mu$m in diameter could be measured. Experiments performed with pure water gave results that were difficult to reproduce and also suggested lower than expected surface tensions. This was consistent with

Liquid	Bo	Oh	Time	Liquid	Bo	Oh	Time
Hexane	0.67	0.0025	1.0903	n-Dodecane	0.59	0.0087	1.17
Hexane	0.65	0.0025	1.00	n-Dodecane	0.29	0.010	1.31
Hexane	0.64	0.0025	1.02	n-Dodecane	0.28	0.010	1.35
Hexane	0.43	0.0028	1.16	n-Dodecane	0.27	0.011	1.41
Hexane	0.076	0.0043	1.38	n-Dodecane	0.075	0.014	1.41
Hexane	0.067	0.0045	1.43	n-Dodecane	0.073	0.015	1.65
Hexane	0.023	0.0059	1.48	n-Dodecane	0.047	0.016	1.63
Toluene	0.38	0.0035	1.23	n-Dodecane	0.047	0.016	1.66
Toluene	0.077	0.0053	1.52	n-Dodecane	0.045	0.016	1.77
Toluene	0.057	0.0057	1.49	n-Dodecane	0.018	0.021	1.75
Toluene	0.048	0.0059	1.75	n-Dodecane	0.018	0.021	1.90
Toluene	0.015	0.008	1.86	n-Dodecane	0.012	0.023	1.74
Toluene	0.006	0.01	1.86	n-Dodecane	0.0051	0.028	2.14

TABLE 1. Representative measurements of pinch off times, non-dimensionalized with $t_n = \sqrt{\rho_i R^3/\sigma}$, of a liquid surrounded by air. We have discarded any measurement with an uncertainty greater that 5 %, corresponding to exceptionally small drops whose radius and pinch off time are difficult to resolve. The drop radii were estimated from recorded high-speed videos. (The corresponding properties used to compute Ohnesorge and Bond numbers are shown in table 1.)

contamination of the water surface, due to its very large surface tension. To avoid surface contamination, measurements were restricted to liquids with low surface tensions, such as toluene, hexane, and n-dodecane. Properties of these liquids found in the literature (Oliviera, Gonzalez & Oliviera 1999; Lide 2002; Tian & Huizhou 2007) are given in table 1.

A 3 ml glass container was rinsed repeatedly with the solutions before filling to avoid contamination. Solutions were frequently discarded over the course of experiments to avoid surface contamination and temperature gradients due to evaporation and the Marangoni effects that could arise from either. The container was filled until the liquid level was slightly above the rim so that the camera could capture images at zero angle. Drops were placed gently on the liquid–air interface with a glass pipette, by hand, using fluid taken from the container. The drops were illuminated from behind through a translucent screen to achieve a silhouetting effect. This provided excellent contrast for drop measurements. Images of the coalescence process were recorded using a Phantom V7 high-speed camera at 47 000 frames per second. Only drops that coalesced with negligible vertical velocity were considered.

5. Results and discussion

5.1. *Validation of the numerical method*

We begin our study by verifying the validity of our numerical simulations. We first focus on the air–water system, water being the inner fluid. The large density and viscosity ratios associated with this system render exact simulations difficult. Using the actual air and water densities yields a density ratio of $\alpha \sim 800$. For such a high value of α, a resolution of approximately 2048×2048 grid points is required, over a 6×6 domain, to ensure mass conservation within a few per cent. However, we note that lower values of α produce essentially the same flow while being much less computationally demanding. For $\alpha > 5$, we have found that our results are virtually independent of the density ratio, as can be seen in figure 3(a) where the evolution

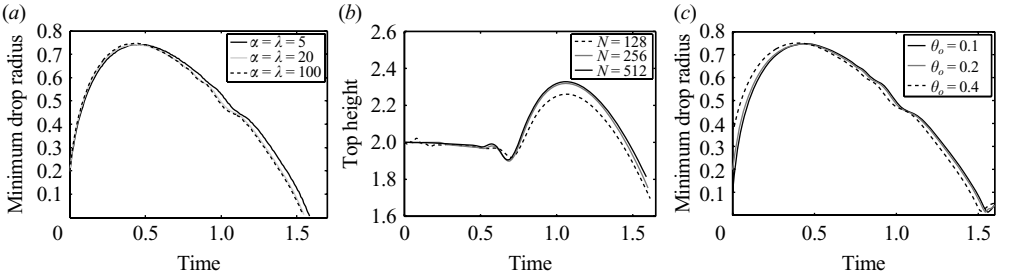

FIGURE 3. (*a*) Time evolution of the neck radius for various density (α) and viscosity (λ) ratios. Once the radius falls below the pinch off threshold, simulations are interrupted and pinch off is considered to have occurred. The number of grid points was $N = 256$ in a 6×6 domain. (*b*) Height of the top of the drop as a function of time for various resolutions, with $\alpha = \lambda = 10$. (*c*) Neck radius as a function of time for various initial opening angle, θ_0, of the connection between the drop and lower reservoir. Parameters used were $Bo = 0.013$, $Oh = 0.0025$.

of the distance to the axis of the drop (neck width) is shown for various values of α and λ. We have therefore elected to simulate air–water systems using $\alpha = \lambda = 10$, corresponding to an air density of 100 kg m^{-3}. This allows us to use a coarser resolution and maintain a computational time of a few hours.

Figure 3(*b*) shows the position of the top of the drop as a function of time for an air–water system resulting in pinch off. While a resolution of 128 grid points is insufficient to adequately capture the motion of the drop, we see that resolutions of 256 and 512 grid points yield nearly identical results before pinch off. In particular, oscillations of the top of the drop due to capillary waves are well resolved in both cases. After pinch off, the two sets of simulations diverged progressively as the recoil of the daughter drop and its bouncing of the reservoir involved smaller length and time scales. Here we focussed on the dynamics of the drop before pinch off is reached and a resolution of 256×256 was therefore sufficient. We also verified that mass and total energy (the sum of kinetic, potential, surface energy and dissipated energy) are conserved to within a few per cent for such a resolution.

We also verified that the choice of the initial width of the neck connecting the drop to the lower reservoir had no influence on the coalescence outcome, provided it was not too wide. We show in figure 3(*c*) the time evolution of the neck width for various initial configurations. The drop is always assumed to be spherical, except for an opening at the bottom where it connects to the reservoir. Varying the angle of the opening, θ_0, within reason, made no difference in the progression of the coalescence process, other than to provide a head start to drops initiated with a larger opening angle.

Finally, we have verified that features that may easily be observed in experiments, such as the radius of the daughter drop, R_d, and the time required for pinch off, t_p, agree well with those obtained in our simulations. For both R_d and t_p, we found good agreement between our simulations, experiments and published data (Charles & Mason 1960*b*; Thoroddsen & Takehara 2000; Chen *et al.* 2006). Therefore, provided a sufficiently fine resolution is used, our simulations allow for the accurate description of the dynamics of motion preceding pinch off.

5.2. *Pinch off mechanism*

The mechanism by which a drop coalescing with a horizontal interface forms a smaller drop has recently been explained (Blanchette & Bigioni 2006). We show in figure 4(*a*)

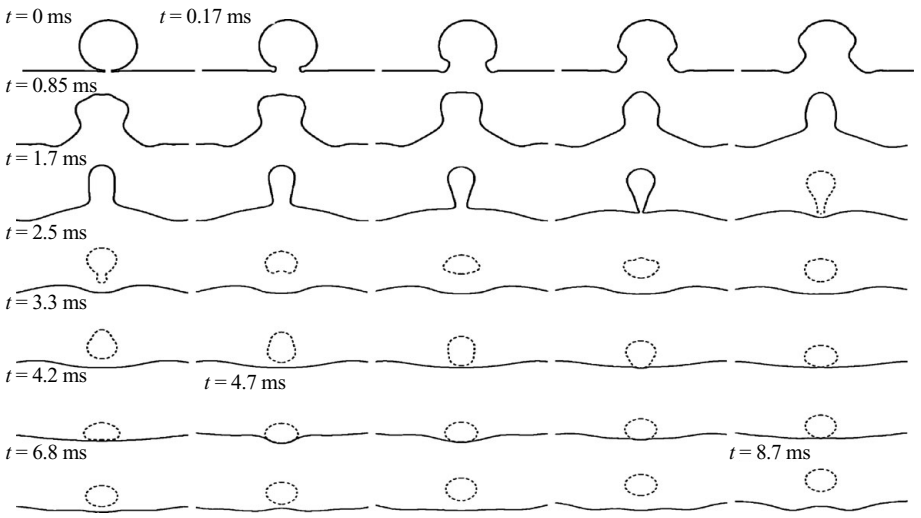

FIGURE 4. Time evolution of the interface of a water drop surrounded by air. The drop is initially at rest and a small neck joins it to the water below the interface. After pinch off, the daughter drop is shown as a dashed line. Here the initial drop radius was 0.5 mm and the corresponding non-dimensional parameters were $Bo = 0.03$, $Oh = 0.0053$, $\alpha = \lambda = 100$.

time sequence of typical simulation results obtained for water drops in air displaying the pinching of a drop. (A corresponding video may be found in the supplementary material at faculty.ucmerced.edu/fblanchette/jfm/dropmovies.html.) Capillary waves generated by the initial expansion of the neck travel upward along the drop's surface and generate oscillations of the top of the drop (see figure 3). These oscillations significantly deform the drop, stretching it vertically to form a nearly cylindrical drop. As the drop is being stretched vertically, surface tension acts to pull the sides of the drop towards the centre. Provided capillary waves have sufficiently delayed the vertical collapse, pinch off will occur and a smaller drop will be left above the interface. If the waves are damped before they reach the summit of the drop, the vertical collapse will overtake its horizontal counterpart and no pinch off will occur. It was found that a significant fraction of the wave amplitude will be dissipated if

$$(Rk)^{3/2}\pi\mu_i/(\sigma\rho_i R)^{1/2} = (Rk)^{3/2}\pi Oh = O(1), \tag{5.1}$$

where k is the dominant wavenumber. In an air–liquid system, a critical value of Oh was found to be approximately 0.026, in the limit of small Bo.

After pinch off, the recoil of the lower part of the daughter drop causes it to oscillate violently as it progresses downward. The downward motion of the drop is mostly due to its velocity at the time of pinch off, as the effect of gravity is comparatively small. Upon hitting the interface, the daughter drop penetrates to a depth approximatively equal to its radius before rebounding.

5.3. *Critical Ohnesorge number*

We used numerical simulations to determine the critical Ohnesorge number as a function of Bond number, density ratio and viscosity ratio. The initial shape and position of the drop and lower surface are obtained in one of two manners. In the simplest case, labelled 'spherical', we consider a spherical drop and a planar surface with a small overlap. Alternatively, we first simulate a drop coming to rest on a horizontal fluid interface. We then use the resulting deformed drop and interface

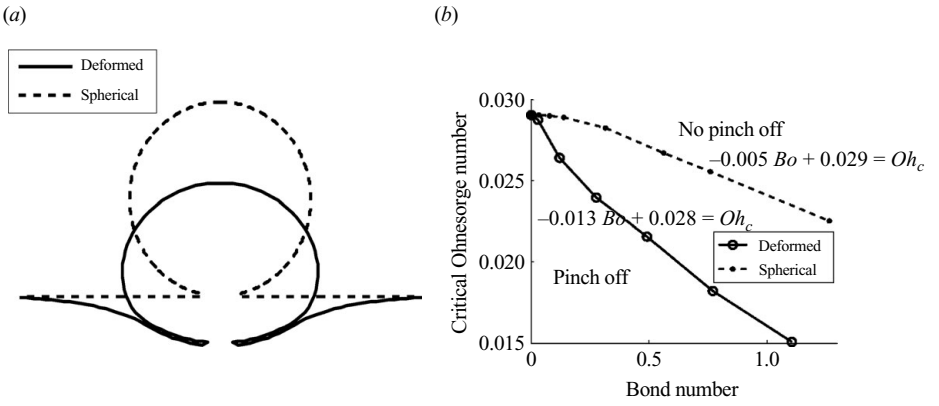

FIGURE 5. (*a*) Initial conditions used for $Bo = 0.5$. The dashed curve shows a spherical drop overlying a flat surface (referred to as 'spherical'). The solid curve shows a drop resting on an interface, both deformed under the influence of gravity (referred to as 'deformed'). (*b*) Critical Ohnesorge number as a function of Bond number in liquid–liquid systems for both sets of initial conditions. Here the fluid viscosities were exactly matched ($\lambda = 1$) and the densities were nearly matched ($\alpha = 1.05$).

position as an initial condition, labelled 'deformed', and initiate coalescence by joining the surface of the drop to that of the bulk fluid (see figure 5). We fix two of the three parameters and select several values of the third. Varying only the Ohnesorge number, we observe that pinch off occurred only for values of Oh below a critical value, Oh_c.

Figure 5(*b*) shows the dependence of Oh_c on Bond number for liquid–liquid systems, where $\alpha = 1.05$ and $\lambda = 1$. A similar plot for gas–liquid systems may be found in Blanchette & Bigioni (2006). In all cases, pinch off is seen to occur at small Oh and Bo. The dependence of Oh_c on the Bond number appears to be relatively weak and linear. Not surprisingly, larger Bond numbers are not favourable to pinch off as they correspond to an increased influence of gravity and thus accelerate vertical collapse. When deformed initial conditions are used, Oh_c is decreased because sagging drops require longer horizontal collapses and shorter vertical collapses. Somewhat surprisingly, both air–liquid and liquid–liquid systems display similar values of Oh_c, with larger values of α and λ corresponding to slightly larger Oh_c.

Focusing on spherical drops of small Bond numbers, we investigate the effect of the fluid density (α) and viscosity (λ) ratios for $\alpha \geqslant 1$ and $\lambda \geqslant 0.3$. As both the inner and outer fluids affect wave dissipation and inertia, we look for an analogue of the critical Ohnesorge number in terms of a weighted viscosity, $\mu_i(1 + b/\lambda)$, and density, $\rho_i(1 + a/\alpha)$, with a and b constants to be determined. Figure 6(*a*) shows that the square of the critical Ohnesorge number depends linearly on the normalized outer density, indicating that the use of a weighted density is appropriate to describe the critical conditions at which partial coalescence occurs. Fitting the numerical data yields $a = 2.22 \pm 0.1$, indicating that the density of the outer fluid is more influential than that of the inner fluid. This may be understood from the consideration that the volume of displaced outer fluid exceeds that of the inner fluid. Similarly, figure 6(*b*) shows that the inverse critical Ohnesorge number scales linearly with the normalized outer viscosity. Fitting the numerical data yields $b = 0.53 \pm 0.1$. Here the inner viscosity appears as most influential, presumably because most of the wave dissipation occurs inside the drop where the fluid motion is constrained to a smaller space.

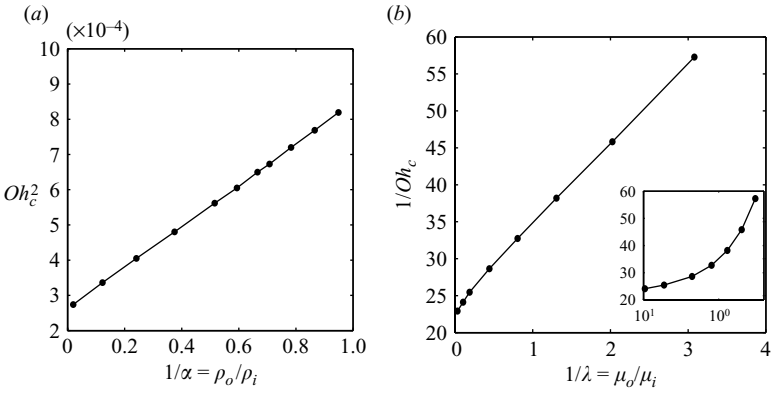

FIGURE 6. (*a*) Critical Ohnesorge number squared as a function of the fluid density ratio in a system of matched viscosities ($\lambda = 1$) and where gravity has a negligible influence ($Bo = 0.02$). (*b*) Dependence of the inverse critical Ohnesorge number on the viscosity ratio in a liquid–liquid system ($\alpha = 1.05$) at low Bond number ($Bo = 0.02$).

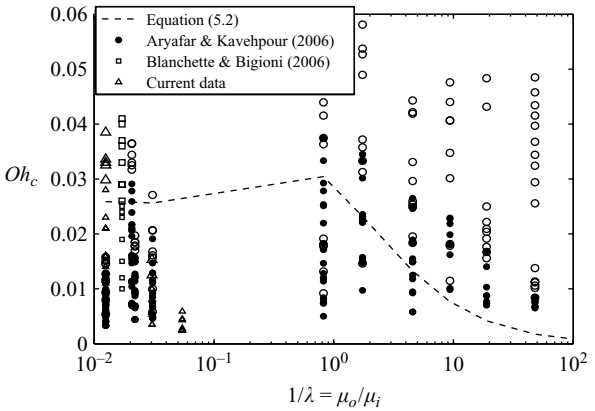

FIGURE 7. Comparison of (5.2) with experimental observations of partial (closed symbols) and total (open symbols) coalescence from different authors. Data was restricted to Bond numbers smaller than 0.1, and the density ratio was set to 1 for liquid–liquid systems and 700 for gas–liquid systems.

An approximate compounded criterion that fits well with all our simulation results is that pinch off occurs if

$$\frac{Oh(1 + 0.53/\lambda)}{\sqrt{1 + 2.22/\alpha}} < 0.026 - 0.013Bo. \tag{5.2}$$

This criterion was obtained for α between 1.05 and 10, λ between 0.3 and 10 and Bo between 0 and 1, all of which were only varied independently. Criterion (5.2) was compared against available data for relatively small Bond numbers as shown in figure 7. In the regime where computations were performed, the agreement between experimental data and (5.2) is found to be good. However, in cases where the outer fluid was more viscous than the inner fluid, $\lambda \leqslant 0.3$, (5.2) appears to underpredict the critical Ohnesorge number. We note that partial coalescence in systems with large outer viscosities were also reported to have markedly different critical Ohnesorge number, pinch off time and radius of the daughter drop (Gilet *et al.* 2007). The

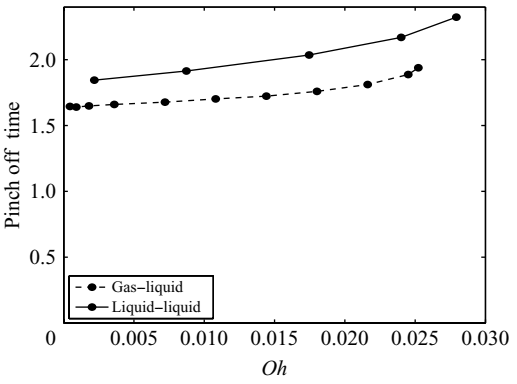

FIGURE 8. Time of pinch off as a function of the Ohnesorge number for spherical drops in liquid–liquid ($\alpha = \lambda = 1$) and gas–liquid ($\alpha = \lambda = 10$) systems. The Bond number here was kept fixed at $Bo = 0.02$.

regime $\lambda < 0.3$ has not been explored in detail here and it is possible that, in this more viscous regime, viscous effects were not properly accounted for at the resolution used in our simulations. Future investigation of this regime thus appears needed.

5.4. *Self-similarity*

Previous authors have observed that multiple coalescence yields a daughter drop with radius R_d almost always half the size of the initial drop and concluded that the pinch off process was independent of drop size, what Thoroddsen & Takehara (2000) refer to as self-similar. We study in this section what aspects of the pinch off process, if any, depend on the drop size.

The fact that the time elapsed between coalescence and pinch off scales as $t_n \sim \sqrt{\rho_i R^3/\sigma}$ was used as an argument supporting self-similarity by Thoroddsen and Takehara (2000). We investigated numerically the dependence of the pinch off time on Bo and Oh for systems with either gas or liquid as an outer fluid. When heavy air was used as an outer fluid, the non-dimensional pinch off time, t_p, was approximately 1.7, in good agreement with previously published experimental results (Thoroddsen & Takehara 2000). Drops with a large Bond number that deformed the interface pinched off faster, with $t_p \sim 1.2$. However, as the onset of coalescence is not well reproduced numerically for drops of large Bond number, we could not investigate this dependence more systematically. The time of pinch off of undeformed (spherical) drops was nearly unaffected by variations in Bond number. On the other hand, increasing the Ohnesorge number partially delayed pinch off and led to values of t_p as large as 1.95 for air–water systems and 2.35 for liquid–liquid systems (see figure 8). In general, the use of a heavier outer fluid slowed down the process of partial coalescence. In agreement with out simulations, experimental measurements of the pinch off time of drops with large Bond numbers were generally faster in non-dimensional units. Measured times were as small as 1.0 for a drop with $Bo = 0.65$ (see table 2). Drops with Ohnesorge numbers closer to Oh_c also had a tendency to pinch off slower, with recorded times as slow as 2.14 for the more viscous fluid *n*-dodecane. In non-dimensional units, small drops, which have large Oh and small Bo, thus tend to pinch off the slowest and large drops the fastest.

For identical initial conditions, i.e. a spherical drop coming into contact with a horizontal surface, figure 9(*a*) shows that the non-dimensional radius of the daughter drop depends only very weakly on both Bo and Oh and remains confined between 0.5

Liquid	Viscosity (cP)	Density ($g\,ml^{-1}$)	Surface tension ($dynes\,cm^{-1}$)
Toluene	0.59	0.87	28.5
Hexane	0.33	0.66	18.4
n-Dodecane	1.44	0.75	26.1

TABLE 2. Properties of fluids used in experiments displaying partial coalescence as found in the literature for a temperature of 20 °C (Oliviera *et al.* 1999; Lide 2002). Note that the viscosity of *n*-dodecane was extrapolated from measurements taken at higher temperatures, 25 °C and 30 °C (Tian & Huizhou 2007).

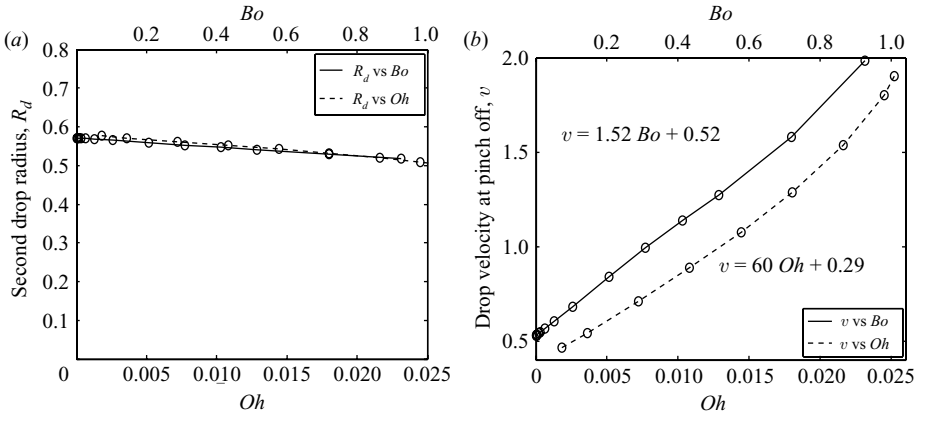

FIGURE 9. Dependence of the non-dimensional daughter drop radius (*a*) and average downward velocity (*b*) on the Bond and Ohnesorge numbers. When varying Bo, we kept $Oh = 0.0038$ fixed; when varying Oh, we kept $Bo = 0.01$ fixed. Here we use a heavy air–water system: $\rho_i = 1.0$, $\mu_i = 0.01$, $\rho_o = 0.1$, $\mu_o = 0.001$. The formulas in (*b*) are linear fits to the numerical data.

and 0.58. Increasing the Ohnesorge number reduces the vertical extent by which the drop is being stretched by capillary waves, resulting in slightly smaller drops, while increasing Bo causes gravity to increase the acceleration of the inner fluid, leaving less fluid to form a daughter drop. Overall though, the daughter drop radius appears nearly constant, in agreement with the observations of Thoroddsen & Takehara (2000). However, when the initial conditions are modified to include the deformation of the drop and of the interface prior to coalescence, large variations are observed in R_d. Large drops, with Bond number of 0.5, for example, are seen to yield daughter drops of radius as low as 0.3. As the drop deforms under the effect of gravity, a larger fraction of its mass ends up below the surface level even before coalescence is initiated. Pinch off therefore occurs higher relative to the centre of the drop and less fluid is left in the daughter drop. These observations are in good agreement with the trend observed by Charles & Mason (1960*a*), where most of the data at low Bond number has a size ratio near 0.5, and that at larger Bond numbers has a size ratio close to 0.3, and were also confirmed in our experiments. We found that large drops, with Bond number as large as 0.8, and relatively small Ohnesorge numbers, of order 0.001, produced daughter drops with radii as small as 0.3. However, it should be emphasized that strongly deformed drops are likely to initiate coalescence away from their symmetry axis and that the initial conditions used here are only approximate.

While our code does not allow us to record the bouncing process accurately, we can nonetheless determine the average non-dimensional downward velocity of the drop at the time of pinch off. Figure 9(*b*) shows that, even with identical initial conditions, the velocity may vary by a factor of 4 with varying Ohnesorge and Bond numbers. This contradicts the assumption of self-similarity of the pinch off process. Not surprisingly, larger Bond numbers accelerate the drop downward, as the effect of gravity pulling on the drop is more readily felt. Increasing the Ohnesorge number also accelerates the drop, which may appear counterintuitive at first since it implies that more viscous systems yield larger drop velocities. However, considering that the vertical acceleration of the drop is mostly due to surface tension pulling down on the top of the drop, which is opposed by the capillary waves rushing upward, explains the influence of Oh. As capillary waves are damped by larger viscous effects, nothing opposes the downward push of surface tension and the drop accelerates further. Therefore, drops that are near the threshold Ohnesorge number will hit the surface with the largest velocity and are thus likely to bounce higher than drops with smaller Oh. These results exhibit the same trend seen in the model developed by Honey & Kavehpour (2006), where larger Ohnesorge number drops were predicted to have greater downward speed through their effect on the size of the daughter drop. Combining their model with that of Aryafar & Kavehpour (2006) for the daughter drop size yields a velocity at pinch off of

$$v = \frac{1}{e}\sqrt{\frac{48}{5}\frac{1}{1-\frac{6}{5}Oh}} + Bo.$$

Compared to our results shown in figure 9(*b*), their model exhibits a similar dependency on Bond number, but a much weaker dependence on Ohnesorge number, observations that presumably result from the fact that their velocity model only takes direct account of gravity and surface forces.

Similar results were observed in liquid–liquid systems where the density ratio was set to $\alpha = 1.05$. The radius of the daughter drop remained fairly constant for various Bond and Ohnesorge numbers, ranging from 0.43 to 0.53. Note that the daughter drops are slightly smaller in liquid–liquid systems than in gas–liquid systems. However, the downward velocity of the daughter drops at pinch off seems to be nearly independent of the outer fluid's density, with values ranging from 0.45 to 1.2 in liquid–liquid systems.

5.5. *Satellite and other droplets*

Over the course of our study, we observed that satellite droplets sometimes formed during the pinch off process, as was also reported for large drops in liquid–liquid systems (Charles & Mason 1960*b*) and gas–liquid systems (Thoroddsen & Takehara 2000). Numerically, we observed that droplets with a large Bond number initiated with deformed interfaces could yield a second daughter drop (see figure 10). While we did not perform a detailed study of when such satellite drops occurred, we noticed that only drops with $Bo > 0.3$ yielded these so-called tertiary droplets in liquid–liquid systems. Gas–liquid systems required even larger values of Bo to exhibit satellite drops. Moreover, if coalescence was initiated while the drop and interface were still undeformed, no satellite drops were observed for any Bond number. This indicates that the initial shape of the drop is determinant in the formation of satellite drops. After pinch off, the satellite drop finds itself caught between the larger daughter drop and the interface. In experiments, the satellite drop did not coalesce with either fluid masses but rather rebounded vigourously as the daughter drop bounced up. The

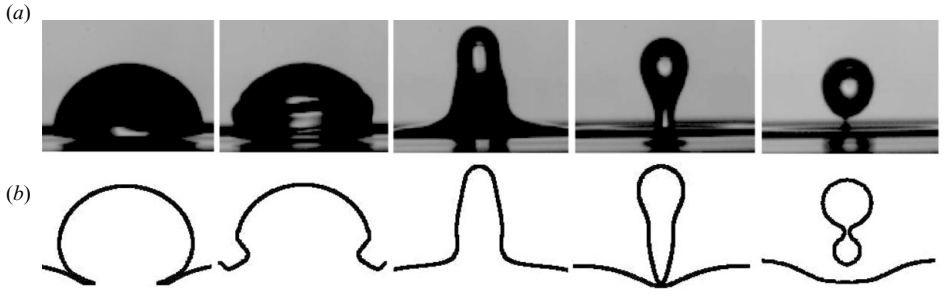

FIGURE 10. (*a*) Sequence of experimental pictures of a drop of hexane with initial radius 0.11 cm ($Bo = 0.43$ and $Oh = 0.0045$). A satellite drop forms after the first pinch off and is temporarily trapped between the daughter drop and the lower reservoir before being ejected to the side. (*b*) Numerical simulations with parameters corresponding to the experimental set-up but with heavy air ($\alpha = \lambda = 10$). Pictures and numerical frames were chosen to emphasize salient features of the flow and are approximately 0.4 ms apart.

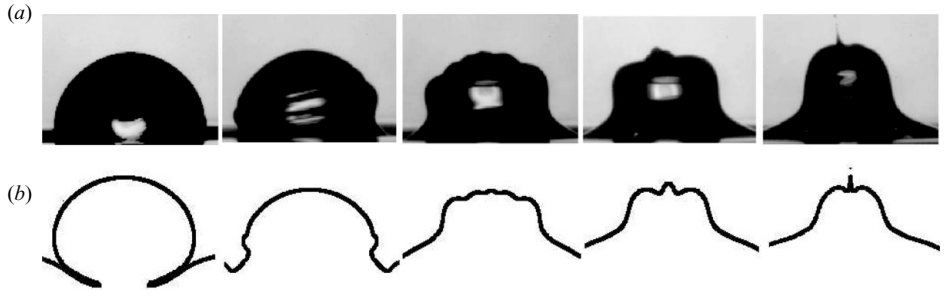

FIGURE 11. (*a*) Experimental pictures of the coalescence of a hexane drop of radius 0.14 cm ($Bo = 0.70$, $Oh = 0.004$) leading to the ejection of a jet of tiny droplets from the top of the drop. (*b*) Numerical simulations with parameters corresponding to the experimental set-up and heavy air ($\alpha = \lambda = 10$). Note that in both experiments and simulations, the surface undergoes one full oscillation of the top surface between the fourth and fifth frames shown. Pictures and numerical frames were chosen to display important stages of the coalescence process and are approximately 0.2 ms apart.

satellite drop usually rebounded at a low angle to the horizontal and with a velocity such that it quickly left the viewing frame of the camera. A typical satellite drop radius was 0.1 times the initial drop radius, in fair agreement with those observed in simulations.

An entirely different kind of tertiary droplet was also observed experimentally for extremely large and deformed drops ($Bo > 0.5$). For sufficiently deformed drops, the convergence of capillary waves at the summit of the drop was sufficiently vigourous to result in the ejection of one or several very small droplets in a nearly vertical direction (see figure 11). Larger drops generated the most vigourous jets of several tiny droplets. Similar jets have been observed in bursting bubbles (Blanchard 1989), but to the best of our knowledge had not been reported in coalescing drops. Unfortunately, the large variation of scale between the initial drop and the ejected droplets did not allow us to fully resolve the ejection of droplets and prevented the convergence of the numerical simulations. Jet ejection at the top of the drop was occasionally observed in our experiments (see figure 11), but we have not found a regime in which such ejection could be reliably observed.

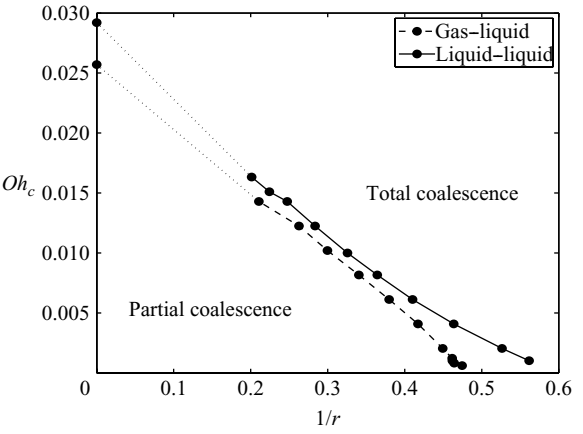

FIGURE 12. Critical Ohnesorge number for partial coalescence of a drop–drop system as a function of the drop size ratio (r = large radius/small radius). The solid line links numerical data and the dotted line is an interpolation towards the point at $1/r = 0$, corresponding to a drop merging with a flat interface. To focus on the effect of the interface's curvature, we neglect gravity: $Bo = 0$. Other parameters are $\lambda = \alpha = 1$ for the liquid–liquid system and $\lambda = \alpha = 10$ for the gas–liquid system.

5.6. *Drop–drop multiple coalescence*

Emulsions consisting of a large number of suspended drops provide an obvious context in which multiple coalescence may occur. With this application in mind, we studied the conditions under which multiple coalescence could occur when two drops of different sizes came into contact. To reduce the parameter space, we restrict our attention to cases where gravity has a negligible effect on the dynamics of motion and set $Bo = 0$. We consider liquid drops surrounded either by a second liquid of matched density and viscosity ($\alpha = \lambda = 1$) or by a gaseous phase ($\alpha = \lambda = 10$). For a given Ohnesorge number, we look for the critical size of the largest drop, while keeping the radius of the smallest drop fixed. We position the larger drop below the smaller one to emphasize the parallel between a flat interface and a drop of infinite radius.

The forces at play during drop–drop coalescence are the same as when a small drop coalesces with a flat interface, with the addition that the larger drop also tends to pull the smaller drop towards its centre. The surface tension of the larger drop generates a downward force of approximate magnitude $\sigma/(rR)$, where r is the ratio of the large to small drop radii and R the radius of the small one. This additional force plays a role similar to that of gravity and accelerates the small drop towards the larger one. Figure 12 shows the critical Ohnesorge number as a function of the ratio of drop sizes, r. The value of Oh_c found for a flat interface, corresponding to $r \to \infty$, is shown as a point on the vertical axis. The data obtained numerically and shown in figures 5 and 12 supports the parallel between gravity (Bond number) and curvature effects of the larger drop ($1/r$). While we did not perform a detailed experimental study of drop–drop coalescence, we have observed the partial coalescence of a small drop with a larger drop in a parameter regime consistent with that described above. We also note that partial coalescence between drops of size ratio $r = 2$ appears to have been observed experimentally by Anilkumar, Lee & Wang (1991) in a regime consistent with those of figure 12, but the authors did not discuss this observation in any detail.

6. Conclusion and outlook

We have developed accurate numerical simulations of the phenomenon of partial coalescence. These simulations have been used to confirm and broaden the scope of experimental results regarding the values of the critical Ohnesorge number for gas–liquid and liquid–liquid systems. The flexibility of the numerical simulations allows the detailed exploration of the effects of gravity, density ratio and viscosity ratio on the partial coalescence process.

Using our numerical model, we were also able to observe the partial coalescence of two drops of different sizes and were able to determine that the minimal radius ratio required to observe partial coalescence is approximately 1.6. The low magnitude of this ratio implies that partial coalescence is likely to occur frequently in dilute emulsions. We have also determined, both numerically and experimentally, that the coalescence of significantly deformed drops may result in the formation of satellite drops and in the ejection of tiny jets, which may be relevant to the formation of mist by breaking waves.

At present, the available simulations are not adaptive in space and therefore have difficulties describing the small scales associated with the final stages of the pinch off process, the drop recoil and the bouncing of the drop on the interface. All of these issues could be addressed by the use of an adaptive grid, which would increase the resolution near the interface. Increased local resolution could also help determine more accurately the conditions under which satellite drops and jets may form, as both of these features occur over small scales and for deformed drops. Despite the current limitations, we have been able to quantify the extent to which partial coalescence is a 'self-similar' process and quantified a previously underestimated dependence of the daughter drop velocity on the fluid viscosity. This dependence may be incorporated in existing models predicting the bouncing of the daughter drop (Honey & Kavehpour 2006).

Our investigation has focused on viscosity ratios μ_i/μ_o of order 1 or larger. The regime of small viscosity ratios has also been observed to yield partial coalescence (Aryafar & Kavehpour 2006; Chen *et al.* 2006; Gilet *et al.* 2007) with different characteristics: pinch off time scaling with viscosity, smaller daughter drops, larger critical Ohnesorge number. While there is abundant evidence of the importance of capillary waves in the inertial regime, these waves are not present in the viscous regime, which indicates that partial coalescence there relies on a different mechanism. Preliminary numerical results did not seem to agree with experiments, which may be due to a lack of resolution of the viscous boundary layer that is expected to play a greater role in this viscous regime. More work is thus needed to provide an understanding of the mechanism allowing partial coalescence to occur in the absence of capillary waves.

Other aspects of realistic partial coalescence have yet to be investigated in detail, either experimentally or numerically. Marangoni effects due to composition, temperature or surfactant concentration differences between the drop and the reservoir, may alter the outcome of the merging process. More importantly for practical applications, the impact velocity of the drop may affect the dynamics of coalescence. The regime of small but non-zero drop velocity (Weber number) has yet to be investigated and needs to be better understood before the relevance of partial coalescence to realistic applications can be assessed. Unfortunately, preliminary results revea that both simulations and experiments are very sensitive to the exact conditions of the thin film of outer fluid separating the drop and the reservoir, and repeatability has been difficult to obtain when considering a non-zero impact velocity.

The authors would like to acknowledge Wendy W. Zhang, Heinrich M. Jaeger and Sidney R. Nagel for enlightening discussions and for providing financial and technical support in the early stages of this project, as well as Eric I. Corwin and Lei Xu for experimental advice. They also thank Professor Kavehpour for sharing some of his data and are also thankful to the James Franck Institute of the University of Chicago for hosting the authors in the first part of this work.

REFERENCES

Anilkumar, A. V., Lee, C. P. & Wang, T. G. 1991 Surface-tension-induced mixing following coalescence of initially stationary drops. *Phys. Fluids* A **3**, 2587–2591.

Aryafar, H. & Kavehpour, H. P. 2006 Drop coalescence through planar surfaces. *Phys. Fluids* **18** (7), 072105.

Bach, G. A., Koch, D. L. & Gonipath, A. 2004 Coalescence and bouncing of small aerosol droplets. *J. Fluid Mech.* **518**, 157–185.

Berry, E. X. & Reinhardt, R. L. 1974 Analysis of cloud drop growth by collection. 3. Accretion and self-collection. *J. Atmos. Sci.* **31**, 2118–2126.

Bhakta, A. & Ruckenstein, E. 1997 Decay of standing foams: drainage, coalescence and collapse. *Adv. Colloid Interface Sci.* **70**, 1–124.

Blanchard, D. C. 1989 The size and height to which drops are ejected from bursting bubbles in sea-water. *J. Geophys. Res.* **94**, 10 999–11 002.

Blanchette, F. & Bigioni, T. P. 2006 Partial coalescence of drops at liquid interfaces. *Nat. Phys.* **2** (4), 254–257.

Briggs, W. L. 1987 *A Multigrid Tutorial*. SIAM.

Brown, D. L., Cortez, R. & Minion, M. L. 2001 Accurate projection methods for the incompressible Navier–Stokes equations. *J. Comp. Phys.* **168**, 464–499.

Burrill, K. A. & Woods, D. R. 1973 Film shapes for deformable drops at liquid–liquid interfaces. 3. Drop rest-times. *J. Colloid Interface Sci.* **42**, 35–51.

Cai, Y. K. 1989 Phenomena of a liquid drop falling to a liquid surface. *Exp. Fluids* **7**, 388–394.

Charles, G. E. & Mason, S. G. 1960*a* The mechanism of partial coalescence of liquid drops at liquid/liquid interfaces. *J. Colloid Sci.* **15**, 105–122.

Charles, G. E. & Mason, S. G. 1960*b* The coalescence of liquid drops with flat liquid/liquid interfaces. *J. Colloid Sci.* **15**, 236–267.

Chen, X., Mandre, S. & Feng, J. J. 2006 Partial coalescence between a drop and a liquid–liquid interface. *Phys. Fluids* **18**, 051705.

Cockbain, E. G. & McRoberts, T. S. 1953 The stability of elementary emulsion drops and emulsions. *J. Colloid Sci.* **8**, 440–451.

Dooley, B. S., Warncke, A. E., Gharib, M. & Tryggvason, G. 1997 Vortex ring generation due to the coalescence of a water drop at a free surface. *Exp. Fluids* **22** (5), 369–374.

Friedlander, S. 2000 *Smoke, Dust, and Haze: Fundamentals of Aerosol Dynamics*. Oxford University Press.

Gilet, T., Mulleners, K., Lecomte, J. P., Vandewalle, N. & Dorbolo, S. 2007 Critical parameters for the partial coalescence of a droplet. *Phys. Rev.* E **75**, 036303.

Gonipath, A. & Koch, D. L. 2001 Dynamics of droplet rebound from a weakly deformable gas–liquid interface. *Phys. Fluids* **13**, 3526–3532.

Gonipath, A. & Koch, D. L. 2002 Collision and rebound of small droplets in an incompressible continuum gas. *J. Fluid Mech.* **454**, 145–201.

Hahn, C. P., Chen, J. D. & Slattery, J. C. 1985 Effects of London-van der Waals forces on the thinning and rupture of a dimpled liquid film as a small drop or bubble approaches a fluid–fluid interface. *AIChE J.* **31**, 2026–2038.

Honey, E. M. & Kavehpour, H. P. 2006 Astonishing life of a coalescing drop on a free surface. *Phys. Rev.* E **73** (2), 027301.

Jayaratne, O. W. & Mason, B. J. 1964 The coalescence and bouncing of water drops at an air/interface. *Proc. R. Soc.* A **280**, 545–565.

Lafaurie, B., Nardone, C., Scardovelli, R., Zaleski, S. & Zanetti, G. 1994 Modelling merging and fragmentation in multiphase flows with SURFER. *J. Comp. Phys.* **113**, 134–147.

Lide, D. R. (Ed.) 2002 *Handbook of Chemistry and Physics* (83rd ed.). CRC Press.

Linton, M. & Sutherland, K. L. 1956 The coalescence of liquid drops. *J. Colloid Sci.* **11**, 391–397.

Longuet-Higgins, M. S. & Cokelet, E. D. 1976 The deformation of steep surface waves on water. I. A numerical method of computation. *Proc. R. Soc. Lond.* A **350**, 1–26.

Mohamed-Kassim, Z. & Longmire, E. K. 2004 Drop coalescence through a liquid/liquid interface. *Phys. Fluids* **16**, 2170–2181.

Neitzel, G. P. & Dell'aversana, P. 2002 Noncoalescence and nonwetting behavior of liquids. *Ann. Rev. Fluid Mech.* **34**, 267–289.

Notz, P. K. & Basaran, O. A. 1999 Dynamics of drop formation in an electric field. *J. Colloid Interface Sci.* **213**, 218–237.

Oliviera, R. C. G., Gonzalez, G. & Oliviera, J. F. 1999 Interfacial studies on dissolved gas flotation of oil droplets for water purification. *Colloid Surf.* A **154**, 127–135.

Orme, M. 1998 Experiments on droplet collisions, bounce, coalescence and disruption. *Prog. Ener. Combust. Sci.* **23**, 65–79.

Osher, S. & Fedkiw, R. P. 2001 Level set methods: an overview and some recent results. *J. Comp. Phys.* **169**, 463–502.

Peyret, R. & Taylor, P. D. 1983 *Computational Methods for Fluid Flow*. Springer-Verlag.

Pikhitsa, P. & Tsargorodskaya, A. 2000 Possible mechanism for multistage coalescence of a floating droplet on the air/liquid interface. *Colloids Surf.* A*: Physiochem. Engng Aspects* **167**, 287–291.

Plateau, J. A. F. 1873 Statique Expérimentale et Théorique des Liquides Soumis aux Seules Forces Moléculaires, Gauthier-Villars.

Popinet, S. & Zaleski, S. 1999 A front tracking algorithm for the accurate representation of surface tension. *Int. J. Numer. Meth. Fluids* **30**, 775–793.

Popinet, S. & Zaleski, S. 2002 Bubble collapse near a solid boundary: a numerical study of the influence of viscosity. *J. Fluid Mech.* **464**, 137–163.

Pozrikidis, C. 1992 *Boundary Integral and Singularity Methods for Linearized Viscous Flow*. Cambridge University Press.

Raes, F., van Dingenen, R., Vignati, E., Wilson, J., Putaud, J.-P., Seinfeld, J. H. & Adams, P. 2000 Formation and cycling of aerosols in the global troposphere. *Atmos. Env.* **34**, 4215–4240.

Rein, M. 1996 The transitional regime between coalescing and splashing drops. *J. Fluid Mech.* **306**, 145–165.

Reynolds, O. 1875 On the action of rain to calm the sea. *Proc. Lit. Phil. Soc. Manchester* **14**, 72–74.

Reynolds, O. 1881 On the floating of drops on the surface of water depending only on the purity of the surface. *Proc. Lit. Phil. Soc. Manchester* **21**, 1–2.

Richard, D. & Quere, D. 2000 Bouncing water drops. *Europhys. Lett.* **50**, 769–775.

Sarpaya, T. 1996 Vorticity, free surface and surfactants. *Ann. Rev. Fluid Mech.* **28**, 83–128.

Scardovelli, R. & Zaleski, S. 1999 Direct numerical simulation of free-surface and interfacial flow. *Annu. Rev. Fluid Mech.* **31**, 567–603.

Sethian, J. A. 1999 Fast marching methods and level sets methods for propagating interfaces. Cambridge University Press.

Sussman, M., Almgren, A. S., Bell, J. B., Colella, P., Howell, L. H. & Welcome, M. L. 1999 An adaptive level set approach for incompressible two-phase flows. *J. Comp. Phys.* **148**, 81–124.

Sussman, M., Smereka, P. & Osher, S. 1994 A level set approach for computing solutions to incompressible 2-phase flow. *J. Comp. Phys.* **114**, 146–159.

Thompson, J. J. & Newall, H. F. 1885 On the formation of vortex rings by drops falling into liquids and some allied phenomena. *Proc. R. Soc. Lond.* **39**, 417–436.

Thoroddsen, S. T. & Takehara, K. 2000 The coalescence cascade of a drop. *Phys. Fluids* **12**, 1265–1267.

Tian, Q. & Huizhou, L. 2007 Densities and viscosities of binary mixtures of tributyl phosphate with hexane and dodecane from (298.15 to 328.15) K. *J. Chem. Engng Data* **52**, 892–897.